JOURNAL OF THERMOPHYSICS AND HEAT TRANSFER
Vol. 13, No. 1, January–March 1999

Evaporative Heat Transfer in a Capillary Structure Heated by a Grooved Block

Q. Liao* and T. S. Zhao†
Hong Kong University of Science and Technology, Clear Water Bay, Kowloon, Hong Kong, People's Republic of China

Experimental results of capillary-driven heat and mass transfer in a vertical rectangular capillary porous structure, heated from a grooved block placed on the top, are reported in this paper. The formation of the liquid–vapor menisci in the vicinity of the downward-facing heated surface provided the capillary-force for the upflow of water in the porous structure. The temperature distributions in both the heating block and porous structure, as well as the induced mass flow rate of water, were measured under different heat flux conditions. The experimental results show that with an increase of the imposed heat flux, the heat transfer coefficient increases to a maximum value and then decreases afterward. It is also found that the liquid–vapor interface moved toward the downward-facing heated surface as the imposed heat flux was increased. The heat transfer mechanisms leading to the maximum heat transfer coefficient and the critical heat flux are explained based on the visual observation of the phase-change behavior and the measured temperature distributions within the porous structure. The effects of particle sizes, the inlet temperature of the subcooled liquid, and the adverse gravity force on the heat transfer characteristics are also examined.

Nomenclature

A_h = total cross-sectional area, m^2
c_p = specific heat, W kg^{-1} k^{-1}
h = heat transfer coefficient of evaporator, W m^{-2} K^{-1}
h_{fg} = latent heat of fluid, J kg^{-1}
K = permeability of porous structure, m^2
k_{eff} = effective thermal conductivity, W m^{-1} K^{-1}
L = thickness of porous structure, m
m'' = mass flow rate, kg m^{-2} s^{-1}
Q = heat transporting from heating block to porous structure, W
q'' = heat flux, kW m^{-2}
r_{eff} = effective radius of porous structure at liquid–vapor interface, m
T = temperature, K
$\bar{T}_p$ = mean temperature over a cross section in porous structure, K
$\bar{T}_w$ = mean temperature of the heating block, K
X, Y = coordinates
Δh = adverse hydrostatic head, m
Δp = pressure drop, Pa/m
ΔT = superheat of the heating block, K
θ = effective contact angle, rad
ν = kinematic viscosity, m^2/s
ρ = density, kg/m^3
σ = surface tension, N/m

Subscripts
c = critical
e = evaporation
i = inlet of porous structure
l = liquid
lv = two-phase zone
o = outlet of porous structure
p = porous structure
s = saturation
v = vapor
w = heating block

Superscripts
$-$ = mean value
$''$ = flux

Introduction

RECENTLY, because of the demand in thermal management of advanced space platforms and military spacecrafts as well as the cooling of electrical and electronic devices, a new heat transfer device, so-called capillary pumped loops (CPL) or loop heat pipes (LHP), has been developed and tested.[1–6] One of the key components in a CPL or a LHP system is a capillary evaporator. A typical capillary evaporator consisting of a porous wick and a grooved heating block is shown in Fig. 1. While heat is added on the top of the porous structure through the grooved block, the liquid contained in the porous structure evaporates in the vicinity of the heated surface. The vapor, produced in the porous structure, flows into the grooves of the heating block and exits there. This physical problem is the subject of investigation in this paper.

Problems involving phase-change heat transfer through porous media have been studied extensively in the past because of their important technological applications.[7] However, most of the previous work have been mainly concerned with forced or natural convection with phase change in a porous medium.[8–12] Furthermore, most of the problems treated by the previous investigators have been confined in boiling heat transfer in a porous medium with a bounded heating boundary. For example, the boiling flow along a vertical heated surface immersed in a porous medium has been analyzed by Parmentier,[8] Cheng and Verma,[9] and Wang and Beckermann.[10] Another typical problem of boiling heat transfer in porous media in the literature is a horizontal layer of finite lateral extent that is heated from below and cooled from above.[11,12]

By comparison, there are two unique features in the present problem. First, the heating boundary is a periodically bounded

Received June 24, 1998; revision received Oct. 8, 1998; accepted for publication Sept. 10, 1998.

*Postdoctoral, Department of Mechanical Engineering; currently at the Department of Thermal Power Engineering, Chongqing University, Chongqing, PRC.

†Assistant Professor, Department of Mechanical Engineering.

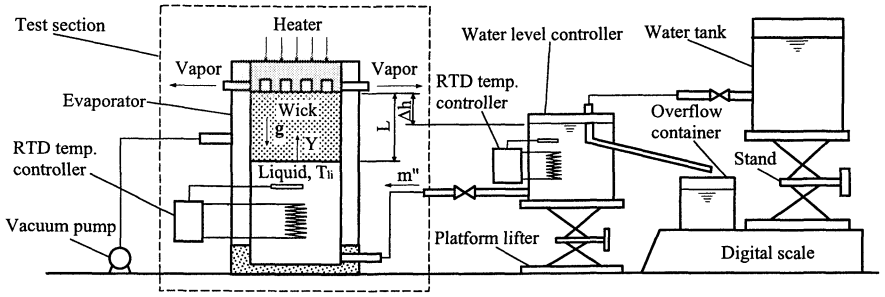

Fig. 1 Schematic of the experimental apparatus.

one (with a number of grooves), which permits the vapor leaving the heating boundary. The second feature of this problem is that the capillary force, developed at the liquid–vapor interface, is the sole driving force of the flow in the porous medium. A review of the literature reveals that the experimental investigation of capillary-driven heat and mass transfer in porous media with this particular boundary condition is scarce, and only a few analyses of the problem have been carried out.

Demidov and Yatsenko[13] numerically investigated the heat and mass transfer processes during evaporation in a wet capillary structure with a rectangular grooved heated wall. They formulated the problem based on two important assumptions. First, they assumed that a superheated vapor zone existed in the vicinity of the heated wall (the groove tip) while the wick was saturated by subcooled liquid elsewhere. Based on this assumption, Darcy's law was applied to the vapor and liquid zones, respectively. They further assumed that, when the vapor zone did not exceed the heated surface, there would be a liquid meniscus near the corners formed by the lateral sides of the fin of the heating block and the top surface of the porous structure. On the other hand, when the vapor zone expanded beyond the surface of the heated wall, this liquid meniscus would disappear. They presented the patterns of isotherms and concluded that the critical heat flux was reached when the expansion of the vapor zone exceeded the area of the heated surface. Khrustalev and Faghri[14] numerically studied the heat and mass transfer processes around a heated triangular solid fin penetrating into a wetted porous structure. They also assumed that the heated surface was surrounded by a vapor zone. They concluded that the critical heat flux for this particular configuration was reached when the increase of the thermal resistance between the heated surface of the fin and the liquid zone with increasing heat flux lead to an extremely high temperature, which is unacceptable in practice; or when the thickness of the vapor zone around the fin tip was equal to the thickness of the porous structure.

In this paper, an experiment was carried out to study the capillary-driven heat and mass transfer processes in a vertical rectangular capillary porous structure, saturated with water and subjected to a grooved heating boundary at the top. The purpose of this work is to understand the heat and mass transfer processes in this particular configuration, providing experimental data for future theoretical investigations. In an attempt to unravel the underlying mechanisms leading to the maximum heat transfer coefficient and the critical heat flux, we visually observed the phase-change behavior in the vicinity of the heated surface and measured the temperature distributions in the porous structure as well. In addition, we also examined the effects of the particle sizes, the inlet temperature of the subcooled liquid, and the adverse gravity force on the heat transfer characteristics.

Theoretical Considerations

To identify the major parameters in the present problem, we shall first present an approximate analysis of the problem under consideration. Consider a rectangular packed-sphere structure of height L with a cross sectional area of $W \times D$, which is heated by a grooved boundary as shown in Fig. 1. The porous structure is initially submerged in a subcooled water, whose level is maintained by an adjacent water reservoir. When the heat flux from the groove boundary is increased beyond a certain value, vaporization begins to take place near the heated surface in direct contact with the porous medium. The vapor produced near the heated surface vents through the groove. A capillary force is developed at the liquid–vapor interface, which induces an upward flow that raises against the gravity and the drag force in the porous structure. A two-phase zone begins to develop near the top of the porous structure. A one-dimensional approximation of force balance in the vertical direction yields

$$\Delta p_c = \Delta p_l + \Delta p_{lv} + \rho_l g \Delta h \tag{1}$$

The first term in the right-hand side of Eq. (1), the pressure drop caused by the liquid flow in the porous structure Δp_l, can be evaluated by Darcy's law as

$$\Delta p_l = m'' \nu_l L_l / K \tag{2}$$

where m'' is the mass flow rate of fluid, L_l is the height of the subcooled liquid phase zone in the porous structure, K is the permeability of the porous structure, and ν_l is the kinematic viscosity of the fluid. The second term Δp_{lv} represents the pressure drop in the two-phase zone, whose explicit expression is difficult to obtain because it depends on several key parameters, including the liquid saturation, the height of the two-phase zone, and the properties of the porous structure. Furthermore, as will be seen from the visual observation described later, the two-phase zone varied not only in the vertical direction, but also in the horizontal direction. For these reasons, we will not attempt to obtain an explicit expression of Δp_{lv} in this work. The third term in the right-hand side of Eq. (1), $\rho_l g \Delta h$, represents the adverse gravity, with Δh being the distance from the top of the porous structure to the liquid level of the working fluid reservoir (referring to as the adverse hydrostatic head). The capillary force Δp_c in the left-hand side of Eq. (1) is given by

$$\Delta p_c = 2\sigma \cos \theta / r_{\text{eff}} \tag{3}$$

where σ is the surface tension, θ is the effective contact angle, and r_{eff} is the effective pore radius of the porous structure. Substituting Eqs. (2) and (3) into Eq. (1), and rearranging yields

$$m'' = (K/\nu_l L_l)[(2\sigma \cos \theta / r_{\text{eff}}) - \rho_l g \Delta h - \Delta p_{lv}] \tag{4}$$

It should be noted that θ, Δp_{lv}, and L_l in Eq. (4) depend on the value of the liquid saturation.

The overall energy balance for the porous structure requires

$$q'' = m''[h_{fg} + c_{pl}(T_s - T_{li}) + c_{pv}(T_{vo} - T_s)] + k_{\text{eff}} \left.\frac{dT}{dY}\right|_{Y=0} \tag{5}$$

where Y is the vertical coordinate measured from the bottom of the porous structure, h_{fg} is the latent heat of vaporization, k_{eff} is the effective thermal conductivity, T_s is the saturation temperature, and the subscripts *li* and *vo* represent the quantities of the liquid at the inlet and the vapor at the groove, respectively. The first term of the right-hand side of Eq. (5) represents the latent heat, whereas the second and the third term represent the sensible heat below and above the saturation temperature, respectively. The last term of Eq. (5) represents the heat loss from the bottom of the porous structure. For the present study of the glass–water system (described in the next section), k_{eff} is relatively small in magnitude, and therefore, the last term is small. In addition, the term $c_{pv}(T_{vo} - T_s)$ is also small because the outlet vapor temperature is very close to the saturated temperature for low to moderate heat fluxes. Neglecting these two terms, Eq. (5) is reduced to

$$q'' \approx m''[h_{fg} + c_{pl}(T_s - T_{li})] \tag{6}$$

Substituting Eq. (4) into Eq. (6), we obtain

$$q'' \approx \frac{K}{\nu_l L_l}\left(\frac{2\sigma\cos\theta}{r_{\text{eff}}} - \rho_l g\Delta h - \Delta p_{lv}\right)[h_{fg} + c_{pl}(T_s - T_{li})] \tag{7}$$

Note that both K and r_{eff} are a function of the particle diameter d_p. Even though the term Δp_{lv} is unknown, Eq. (7) clearly indicates that for given thermophysical properties of fluid and solid, the major parameters that influence the present heat and mass transfer problem are the particle size d_p, the height of the porous structure L, the adverse hydrostatic head Δh, and the inlet fluid temperature T_{li}. As we shall see, the preceding analysis is useful in the design of the experimental setup and the interpretation of experimental data.

Experimental Apparatus and Procedures

The experimental apparatus used in the present investigation is shown in Fig. 1, which consisted of two major parts: the liquid supply system and the test section. As shown in Fig. 1, the liquid supply system consisted of a water tank, a water-level controller, and an overflow container. The deionized water draining from the water tank was bifurcated into two streams in the water-level controller: one stream was directed toward the test section while the remainder was directed toward the overflow container. As such, the water level in the water-level controller could be kept constant during the experiments. The adverse hydrostatic head Δh (the distance between the top of the porous structure and the water level) was controlled by adjusting the elevation of the platform lifter, on which the water-level controller was placed. An RTD controller with a 1.5-kW heater was installed to keep the fluid temperature in the water-level controller to a desired value. Both the water tank and the overflow container were placed on a digital scale such that the mass flow rate flowing to the test section could be measured by reading the mass change per unit time.

A schematic of a rectangular test section is illustrated in Fig. 2. The vertically oriented test section was packed with glass beads. It consisted of four vertical walls: three Teflon® plates located in both the lateral and back sides, and a transparent plate (made of Pyrex®) located in the front side. The phase-change behavior within the porous structure could be observed via the transparent front plate. A perforated plate was installed at the bottom of the test section to hold the glass beads in place during the experiments. The height of the porous structure (Y direction) was adjusted by changing the location of the perforated plate, whereas the other two dimensions of the porous structure were fixed at 99 mm in width (X direction) and 28 mm in depth (perpendicular to the X–Y plane). A grooved copper block (shown in Fig. 3) with a stainless-steel film (0.1 mm in thickness) serving as a heater, a mica sheet serving as an electrical insulator, and a Teflon cover plate serving as a heat insulator on the top, was placed on the top of the porous structure. This heating unit was carefully mounted on the top of the porous structure such that the grooved block fins were in good contact with the porous medium. Owing to the capillary force generated at the liquid–vapor interface near the heated surface, the subcooled liquid was induced to enter the test section from its bottom and flowed upward by overcoming the gravity and drag forces in the porous medium. Vapor, produced near the heated surface, vented into the grooves and exited to the ambient via the vapor tube. The inlet temperature of fluid was well controlled by an RTD temperature controller with two 50-W heaters located in the lower portion of the test section. Both the top and bottom boundaries of the test section were insulated using glass fiber wool, whereas the vertical boundaries were well insulated by a vacuum vessel made of Plexiglas® plates. The vacuum status was kept by a vacuum pump during the experiments.

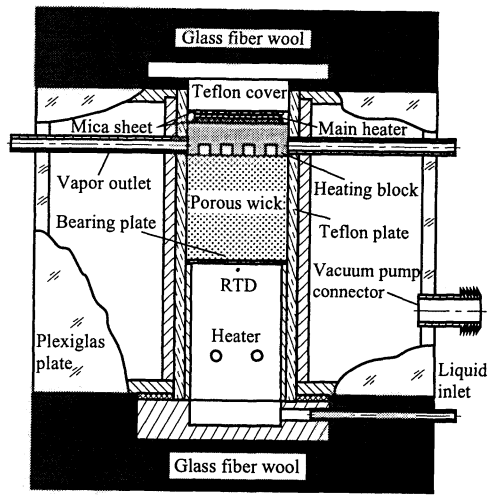

Fig. 2 Schematic of the test section.

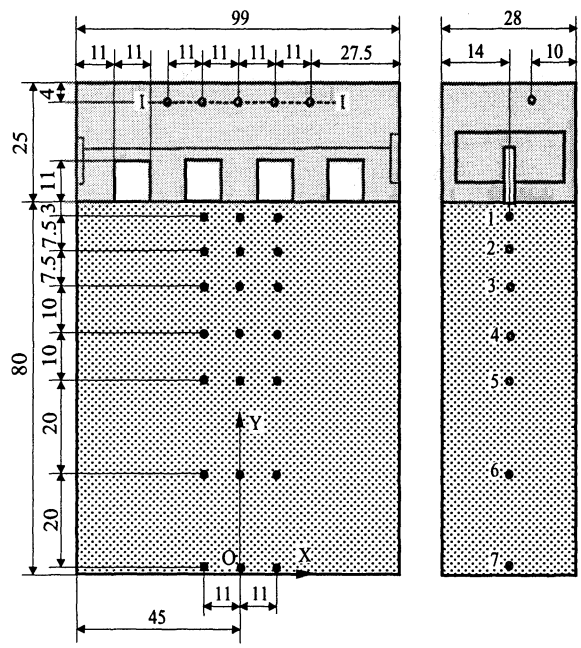

Fig. 3 Arrangement and the locations of thermocouples.

The locations of various thermocouples are shown in Fig. 3. Four T-type thermocouples, 0.8 mm in diameter, were used to measure the temperatures of the heating block, whereas 18 T-type thermocouples, 0.8 mm in diameter, were inserted in

the porous media for measuring temperature distributions in the porous structure. A data-acquisition system, consisting of a personal computer, an A/D converter board (MetraByte DAS-20), and two universal analog input multiplexers (MetraByte EXP-20), was employed to record the temperature measurements.

In the present study, the heat transfer coefficient is defined as

$$h = Q/A_h(\bar{T}_w - T_s) \tag{8}$$

where Q is the heating power, and A_h denotes the heating surface area, i.e., the cross-sectional area of the cooper block. In Eq. (8), $\bar{T}_w$ is the mean temperature of heating block that was obtained by averaging the readings of the thermocouples located along the top of grooved block (I–I), as illustrated in Fig. 3.

To stabilize the boiling conditions and degas the air from the porous structure, prior to each experiment, the water level of the water-level controller was adjusted slightly to the top of the porous structure and a moderate heat flux was provided to keep at boiling temperature at the top of porous structure for 2 h. Then, the water level was adjusted to the required elevation. For each test case, it took about $\frac{1}{2}$ to 1 h for the system to be stabilized. The experimental data were collected under steady-state conditions.

The three physical parameters measured during the experiments were the temperatures of the heating block and the porous medium, the mass flux of water, as well as the imposed heating load. The thermocouples were calibrated to ensure the accuracy within ±0.2°C. It was estimated that the uncertainty of the mass flux was ±0.4%, whereas the uncertainty of the imposed heat loading was ±8.5%, which was primarily caused by the heat loss. Using the uncertainty estimation method of Kline and McClintock,[15] it was estimated that the uncertainty of the heat transfer coefficient was 11.7%.

Results and Discussion

In the present study, four different sizes of spherical glass beads, including 0.50–0.60 mm, 1.00–1.18 mm, 1.98–2.00 mm, and 2.36–2.75 mm, were tested. The averaged diameters of each size (such as d_p = 0.55, 1.09, 1.99, and 2.56 mm) are used to label curves in a subsequent discussion. The same heating block was used for all of the tests. Experiments were carried out by increasing the heat flux from 7 to 370 kW/m^2 for two different heights of the porous structure (80 and 35 mm); three different inlet temperatures (50, 70, and 80°C); and three adverse hydrostatic heads (5.0, 30.0, and 50.0 mm), respectively. In the following, we first present our general observations to the problem under consideration. We then examine and discuss the effects of various parameters, such as particle diameters d_p, the height of the porous structure L, the inlet temperature of fluid T_{li}, and the adverse hydrostatic head Δh, on the heat transfer characteristics.

General Observations

A typical variation of the heat transfer coefficient, as defined in Eq. (8), vs the imposed heat flux for Δh = 5 mm and T_{li} = 80°C, is presented in Fig. 4, where the letter labels represent the corresponding phase-change behavior illustrated in Fig. 5. It is shown that with an increase of heat flux, the heat transfer coefficient increases to a maximum value and then decreases afterward. This interesting phenomenon can be explained based on our observations of the phase-change behavior occurring in the vicinity of the heated surface. A typical sequence of the events are sketched in Fig. 5. At a certain value of the imposed heat flux, e.g., at point a in Fig. 4, nucleate boiling took place at the heated surface of the block. As a result, a number of small dispersed bubbles were continuously generated in the porous medium below the heated surface, as shown in Fig. 5a. Part of these bubbles migrated downward in the

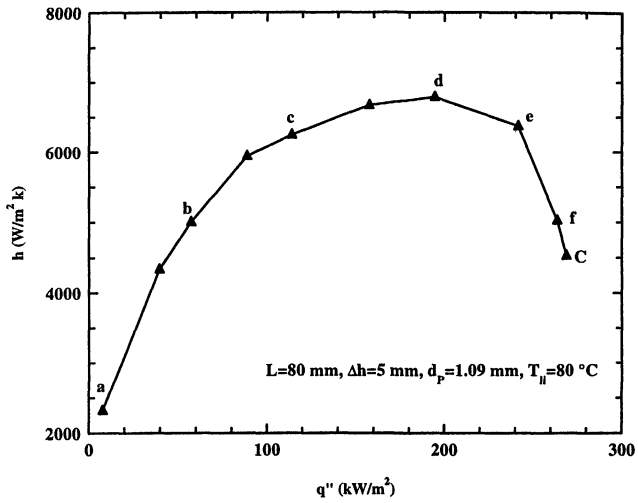

Fig. 4 Variation of the heat transfer coefficient vs the imposed heat flux (where C represents the critical heat flux point).

porous structure as a result of higher vapor pressure adjacent to the heated surface. Some of these bubbles were condensed into liquid in the low-temperature zone, whereas the reminder were vented into the vapor groove. As the imposed heat flux was increased further, both the number of bubbles and the frequency of bubble collisions were increased. As a consequence, a coalesced bubble formed below the heated fin, which grew, and eventually spurted into the vapor grooves from the lateral sides of the heated fin by high-pressure pulses. Subsequently, the liquid was replenished to the heated surface, again owing to the capillary action, and another cycle of bubble generation, coalesce, and collapse began. It was observed that such a cyclic process of bubble collapse and liquid replenishment occurred at a very high frequency. Under the condition of constant heat flux, this coalesced bubble below the heated surface was virtually a bubble and liquid coexisting zone, i.e., a two-phase region, as depicted in Fig. 5b (corresponding to point b in Fig. 4). It is important to note that as the heat flux was increased, this two-phase zone expanded laterally, but at the same time shrank vertically, as shown in Figs. 5c–5e (corresponding to points c to e in Fig. 4). The reduction in the depth of the two-phase zone can be explained as follows: as indicated in Eq. (6), the induced mass flux of the working fluid was increased with the increase of the heat flux. Thus, more subcooled liquid was moving toward the heated surface. As a result, more bubbles in the two-phase zone were condensed into liquid; therefore, the depth of the two-phase zone was reduced. It was found that heat transfer coefficient under the conditions shown in Figs. 5a–5e was increased with increasing heat flux because of the increased cyclic frequency. However, when the imposed heat flux was further increased, the bubbles below the heated surface disappeared and the lateral surfaces of the fin became dry. In this case, only a dry vapor film existed at the interface between the heated surface and the porous structure, as shown in Fig. 5f (corresponding to point f in Fig. 4). Under this situation, heat was transferred to the evaporating front within the porous structure via the vapor film. The lower thermal conductivity of the vapor film led to a smaller heat transfer rate. This is why the heat transfer coefficient shown in Fig. 4 begins to drop beyond a certain value of heat flux. It should be noted that after heat transfer coefficient reached a maximum value, its value was reduced gradually instead of a sharp drop with increasing heat flux. This is because the vapor film existed only below the heated surface in contact with the porous medium, whereas the heat transfer rate in the remainder of the surface of the porous structure was still high. However, when the imposed heat flux was further increased to a critical value, i.e., when the vapor film extended

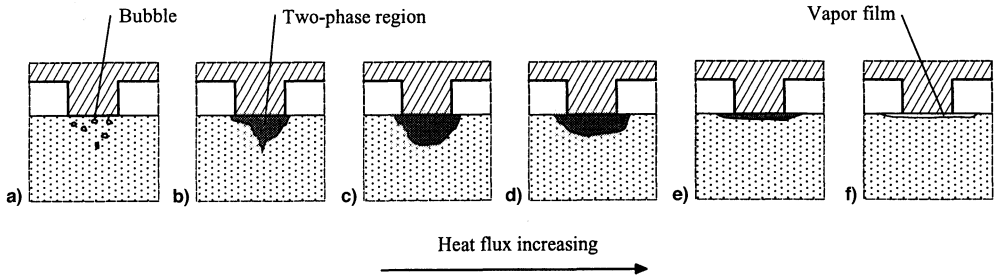

Fig. 5 Observations to the phase-change events below the heated surface when the heat flux was increased.

laterally and eventually covered the entire top surface of the porous structure. Under this situation, the wall and outlet temperatures increased drastically and the steady state could not be maintained. During the experiments, we observed that when the heat flux was increased from $q'' = 268.9$ to 274.3 kW/m^2 (an increase of only 1.9%), the wall and outlet vapor temperatures increased exponentially with time. Therefore, the value of $q'' = 268.9$ kW/m^2 can be regarded as the critical heat flux under this particular condition, as labeled as point C in Fig. 4. It should be mentioned that in some of the subsequent figures, the label C refers to the critical heat flux point under various conditions.

The variations of the temperatures in the porous structure along the vertical direction (Y axis) at three different horizontal locations ($X = -11$, 0, and 11 mm, as shown in Fig. 3), for the inlet liquid temperature of 50°C and the adverse hydrostatic head $\Delta h = 5$ mm, are presented in Fig. 6. It is seen that the temperatures at any horizontal locations ($X = -11$, 0, or 11 mm), under the condition of a lower heat flux ($q'' = 39.6$ kW/m^2), represented by dashed curves, increased along the Y axis from the bottom at the inlet temperature (50°C) to the top of the porous structure, where it was heated by the grooved copper block. A comparison of the temperatures at different horizontal locations shows that the temperatures at $X = 0$ mm are higher than those at $X = -11$ and 11 mm along the Y axis, whereas the temperatures at $X = -11$ and 11 mm were quite close to each other. This is because the thermocouples at $X = 0$ were located just below the heated surface, whereas the thermocouples at $X = -11$ and 11 mm were located below the grooves (see Fig. 3). As the imposed heat flux is increased to $q'' = 268.9$ kW/m^2, however, the temperature variations (represented by the solid curves in Fig. 6) along the Y axis in the lower portion of the porous structure became relatively small, but in the upper portion, the temperature variation became extremely steep. This is because at a low heat flux only a small amount of water evaporated at the top of the porous structure and the induced mass flow rate of the working fluid was relatively small. Thus, the heat convection caused by the corresponding movement of the working fluid was relatively small for this case. However, as the heat flux was increased, more water evaporated and the motion of the water in the porous medium became much more significant, owing to the capillary-driven force at the liquid–vapor interface. Under this situation, convection became more pronounced. Therefore, the temperatures increased relatively slowly in the lower portion of the porous wick evaporator as a result of the cooling effect of the subcooled liquid entering the structure from the bottom, whereas it increased more rapidly in the upper portion of the porous structure because of the heating effect from the top of the structure. This result is in agreement with the our visual observation on the movement of the liquid–vapor interface, i.e., the two-phase zone was reduced with increasing the heat flux. It is also worth noting that the temperature differences between different horizontal locations became smaller at a higher heat flux (solid lines).

The variations of the cross-sectional mean temperature along the Y axis at various heat fluxes are illustrated in Fig. 7. It is interesting to note that the cross-sectional mean temperature at

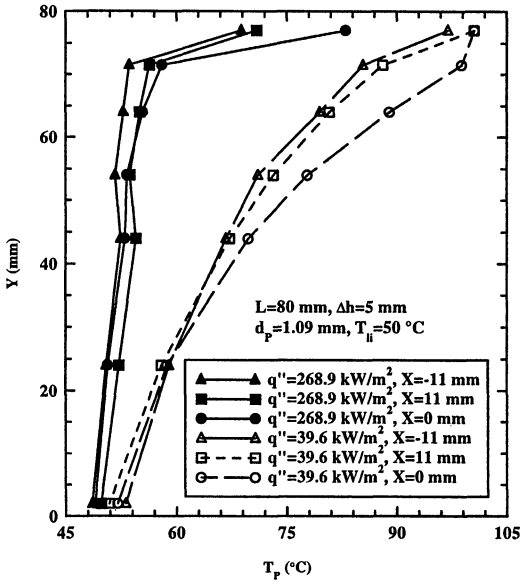

Fig. 6 Variations of temperatures along Y axis at $X = -11$, 0, and 11 mm for different heat fluxes.

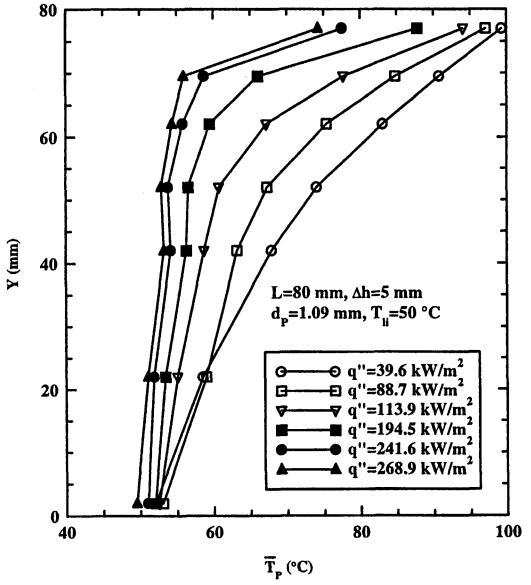

Fig. 7 Effect of the heat flux on the cross-sectional mean temperature variations along Y axis.

each row decreased with the increase of the heat flux. This is one of the unique features of the capillary-driven heat transfer process under consideration. As indicated in Eq. (6), the mass flow rate is coupled with the heat flux. A higher heat flux leads to a higher mass flow rate. Therefore, more subcooled liquid entered the porous structure and cooled the majority portion of the porous structure, except near the top. The temperatures

measured by the thermocouples in the top row (3 mm away from the heated surface, as seen in Fig. 3) were always lower than the saturation temperature of fluid (100°C) in all the tests. This indicates that a dry vapor region corresponding to the critical heat flux must have occurred above this level. These phenomena are consistent with our visual observation, as discussed earlier.

Effect of Particle Sizes

The effect of the particle sizes on the heat transfer coefficient for Δh = 30 mm and L = 35 mm is presented in Fig. 8. It is seen under this particular condition, both the maximum heat transfer coefficient and the critical heat flux (represented by the symbol C) increased substantially as the particle diameter was decreased from d_p = 1.99 mm to d_p = 1.09 mm. This is because the capillary force generated at the interface of the heated surface and the porous structure is increased with the decrease of the particle diameters. A larger capillary force induced more liquid toward the interface of the heated surface and the porous structure, thus enhancing heat transfer. However, as the particle diameter was further reduced to 0.55 mm, the critical heat flux increased, even though the heat transfer coefficient was reduced. The primary reason leading to the reduction of the heat transfer coefficient was that the permeability was very small as the particle diameter became too small. Therefore, the mass flow rate was reduced, implying that only a small amount of liquid could be provided to the interface of the heated surface and the porous structure. The reason that the critical heat flux was increased with decreasing particle sizes was because the capillary force was inversely proportional to the particle size, as indicated in Eq. (3). The porous structure packed with small-diameter beads provided a larger capability of liquid replenishment at the heated surface. Therefore, the small particle size had a higher critical heat flux. It should be pointed out that when the adverse hydrostatic head is reduced to a small value, the effect of the particle diameters will become insignificant because the capillary force plays less of a role in this situation. This was observed in our experiments when the adverse hydrostatic head was reduced to 5 mm.

From the experimental data, we also found that the depth of the two-phase zone was reduced as the particle diameter was reduced from d_p = 1.99, 1.09–0.55 mm. These observations were consistent with the temperature measurements, as shown in Fig. 9. It is seen from Fig. 9 that the cross-sectional mean temperatures near the top region decreased with the decrease of the particle diameter, indicating that the depth of the two-phase zone became smaller.

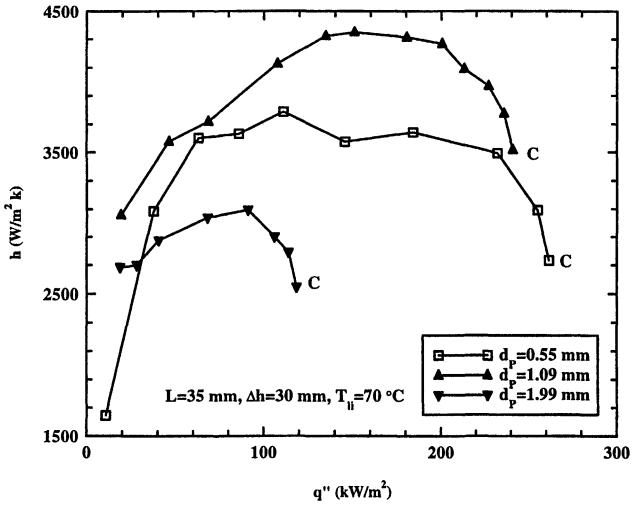

Fig. 8 Effect of the particle sizes on the heat transfer coefficient at different adverse hydrostatic heads Δh (where C represents the critical heat flux point).

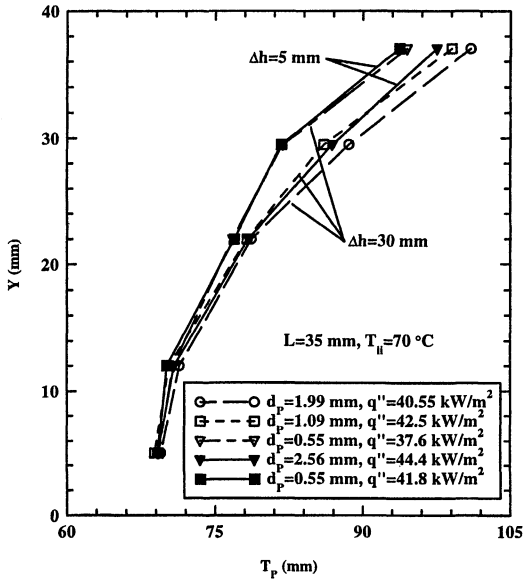

Fig. 9 Effect of the particle diameters on the cross-sectional mean temperature profiles along Y axis.

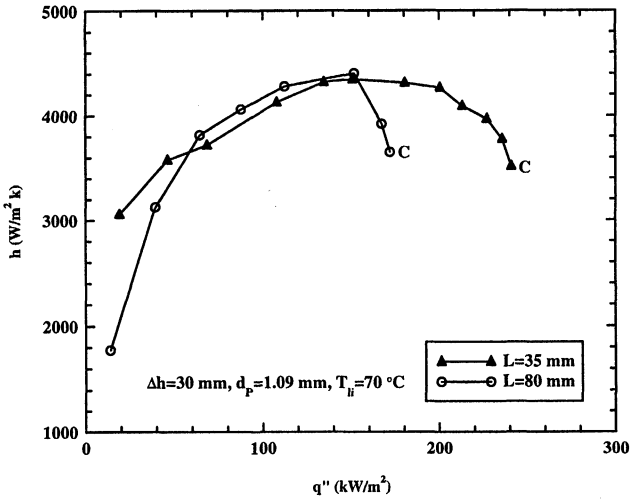

Fig. 10 Effect of the height of the porous structure on the heat transfer coefficient (where C represents the critical heat flux point).

Effect of the Height of the Porous Structure

Figure 10 shows the variation of the heat transfer coefficient for different heights of the porous structure for the same size of particles (d_p = 1.09 mm) and the same adverse hydrostatic head (Δh = 30 mm). It is seen that the critical heat flux for the thinner porous structure (L = 35 mm) is higher than that of the thicker one (L = 80 mm), even though the maximum heat transfer coefficients remain more or less the same. This is because the same capillary force, generated by the same particle size, has to overcome a larger drag force for a thicker porous structure, leading to a decrease of the mass flow rate, and thus, to a decrease in the critical heat flux. Therefore, it can be concluded that a thinner porous structure gave a higher critical heat flux. However, the height of the porous structure has a small effect on the maximum value of the heat transfer coefficient.

Effect of the Inlet Temperature

The effect of the inlet temperature on the heat transfer coefficient for the same porous structure with the same particle size at the adverse hydrostatic head Δh = 30 mm is illustrated in Fig. 11. It is noted from Fig. 11 that both the heat transfer

coefficient and the critical heat flux were substantially increased as the inlet temperature was increased from 50°C to 80°C. The increase of the heat transfer coefficient caused by the increase of the inlet temperature can be explained by the cross-sectional mean temperature distribution shown in Fig. 12. It is seen from this figure that with the same heat flux the temperature near the top was reduced (comparing the solid and the dashed curves) as the inlet temperature was reduced, implying that the two-phase zone increases for a higher inlet temperature. A larger two-phase zone means a larger evaporation surface; therefore, the heat transfer is enhanced. During the experiments, we also found that when the adverse hydrostatic head was reduced to 5 mm, the effect of the inlet temperature became weaker. This is because as the adverse hydrostatic head is reduced, more liquid is available to supply the two-phase zone and the increase of the two-phase zone resulting from the increase of the inlet temperature will lead to a higher heat transfer coefficient.

Effect of the Adverse Hydrostatic Head

The effect of the adverse hydrostatic head on the heat transfer coefficient for the same thickness of the porous structure

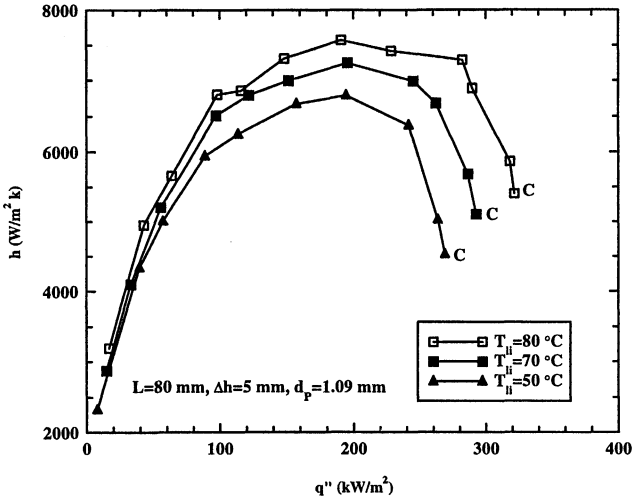

Fig. 11 Effect of the inlet temperature on the heat transfer coefficient at Δh = 5 and 30 mm (where C represents the critical heat flux point).

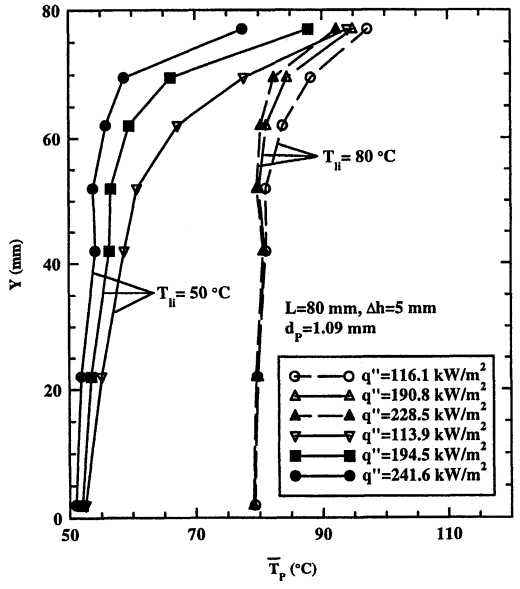

Fig. 12 Effect of the inlet temperature on the cross-sectional mean temperature profiles along *Y* axis for different heat fluxes.

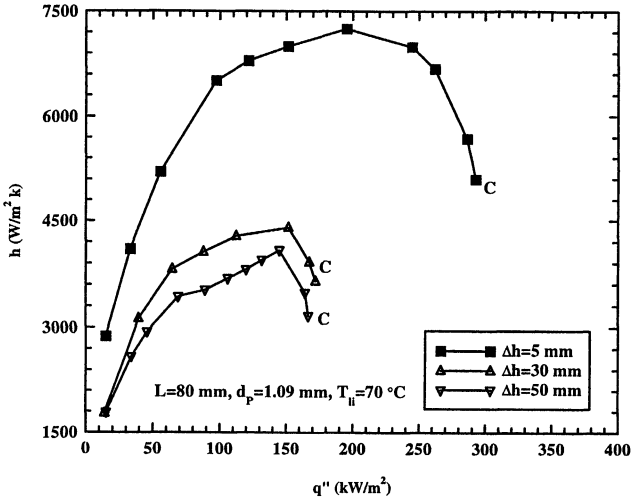

Fig. 13 Effect of the adverse hydrostatic head Δh on the heat transfer coefficient for different particle diameters (where C represents the critical heat flux point).

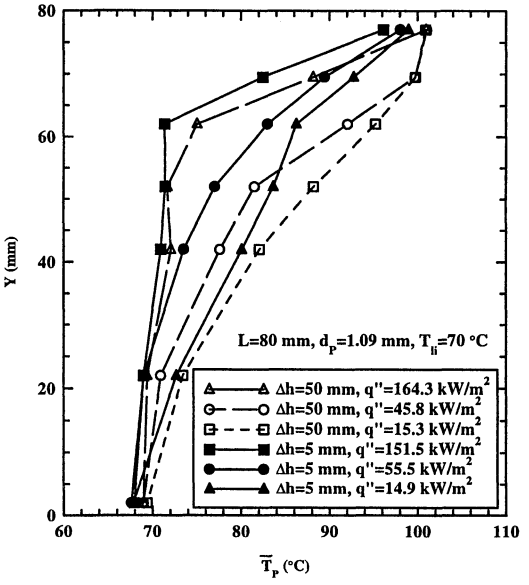

Fig. 14 Effect of the adverse hydrostatic head on the cross-sectional mean temperature profiles along *Y* axis for different heat fluxes.

(L = 80 mm) with the same particle size (d_p = 1.09 mm) and at the same inlet temperature (T_{li} = 50°C) is shown in Fig. 13. It is seen that both the heat transfer coefficient and the critical heat flux were increased with the decrease of the adverse hydrostatic head from 50 to 5 mm. This is because more liquid is supplied to the heated surface for a smaller adverse hydrostatic head. For the same reason, as shown in Fig. 14, the cross-sectional mean temperature near the top of the porous structure is increased with the increase of the adverse hydrostatic head, indicating that the two-phase zone for a higher adverse hydrostatic head is larger.

Conclusions

In this paper, we have presented the experimental results on evaporative heat transfer characteristics in a rectangular capillary porous structure heated by a grooved copper block at the top. Based on the experimental data, the following conclusions may be drawn from this study:

1) With the increase of the imposed heat flux, the heat transfer coefficient increases to a maximum value and then decreases afterward.

2) As the imposed heat flux is increased, the liquid–vapor interface moves toward the heated surface. The critical heat flux is reached when the vapor film expands to cover the whole area of the heated surface. Under this situation, both the wall and the outlet temperatures would increase sharply with the advance of time.

3) For large adverse hydrostatic heads, there exists an optimum particle size for the maximum heat transfer coefficient. The critical heat flux is shown to increase with the decrease of particle sizes. For small adverse hydrostatic heads, however, the influence of the particle size on both the heat transfer coefficient and the critical heat flux becomes less significant.

4) The height of the porous structure is shown to have a large effect on the critical heat flux, but it has a small effect on the maximum value of the heat transfer coefficient.

5) Both the heat transfer coefficient and the critical heat flux increase with the increase of the inlet fluid temperature.

6) The adverse hydrostatic head has a substantial effect on both the heat transfer coefficient and the critical heat flux. A lower adverse hydrostatic head gives a higher heat transfer coefficient and a higher critical heat flux.

Acknowledgment

This work was supported by Hong Kong RGC Earmarked Research Grant HKUST 809/96E. The authors are grateful to Ping Cheng for his valuable suggestions on improving this paper.

References

[1]Ku, J., "Overview of Capillary Pumped Loop Technology," *Proceedings of the ASME 29th National Heat Transfer Conference*, HTD-Vol. 236, Atlanta, GA, 1993, pp. 1–17.

[2]Faghri, A., *Heat Pipe Science and Technology*, Taylor and Francis, Washington, DC, 1995, pp. 578–624.

[3]Chalmers, D. R., Pustay, J. J., Moy, C. B., and Kroliczek, E. J., "Application of Capillary Pumped Loop Heat Transport Systems to Large Spacecraft," AIAA Paper 86-1295, 1986.

[4]Dickey, J. T., and Peterson, G. P., "Experimental and Analytical Investigation of a Capillary Pumped Loop," *Journal of Thermophysics and Heat Transfer*, Vol. 8, No. 3, 1994, pp. 602–607.

[5]Allen, J. S., and Hallinan, K. P., "A Study of the Fundamental Operation of a Capillary Driven Heat Transfer Device in Microgravity," National Heat Transfer Conf., Baltimore, MD, Aug. 1997.

[6]Deng, Q., Ma, T., Zhang, Z., and Wang, J. "Experimental Investigation on the Performance of Evaporator for Capillary Pumped Loops," *Journal of Engineering Thermophysics*, Vol. 19, No. 3, 1998, pp. 330–334.

[7]Wang, C. Y., and Cheng, P., "Multiphase Flow and Heat Transfer in Porous Media," *Advances in Heat Transfer*, Vol. 30, Academic, New York, 1997, pp. 93–196.

[8]Parmentier, E. M., "Two-Phase Natural Convection Adjacent to a Vertical Heated Surface in a Permeable Medium," *International Journal of Heat and Mass Transfer*, Vol. 22, 1979, pp. 849–855.

[9]Cheng, P., and Verma, A. K., "The Effect of Subcooled Liquid on Film Boiling About a Vertical Heated Surface in a Porous Medium," *International Journal of Heat and Mass Transfer*, Vol. 24, No. 7, 1981, pp. 1151–1160.

[10]Wang, C. Y., and Beckermann, C., "A Two-Phase Mixture Model of Liquid-Gas Flow and Heat Transfer in Porous Media. Part II: Application to Pressure-Driven Boiling Flow Adjacent to a Vertical Heated Plate," *International Journal of Heat and Mass Transfer*, Vol. 36, No. 11, 1993, pp. 2759–2768.

[11]Ramesh, P. S., and Torrance, K. E., "Boiling in a Porous Layer Heated from Below: Effects of Natural Convection and a Moving Liquid/Two-Phase Interface," *Journal of Fluid Mechanics*, Vol. 257, 1993, pp. 289–309.

[12]Sondergeld, C. K., and Turcotte, D. L., "An Experimental Study for Two-Phase Convection in a Porous Medium with Applications to Geological Problems," *Journal of Geophysics Resources*, Vol. 82, 1977, pp. 2045–2053.

[13]Demidov, A. S., and Yatsenko, E. S., "Investigation of Heat and Mass Transfer in the Evaporation Zone of a Heat Pipe Operating by the 'Inverted Meniscus' Principle," *International Journal of Heat and Mass Transfer*, Vol. 37, 1994, pp. 2155–2163.

[14]Khrustalev, D., and Faghri, A., "Heat Transfer in the Inverted Meniscus Type Evaporator at High Heat Fluxes," *International Journal of Heat and Mass Transfer*, Vol. 38, 1995, pp. 3091–3101.

[15]Kline, S. J., and McClintock, F. A., "Describing Uncertainties in Single-Sample Experiments," *Mechanical Engineering*, Vol. 75, Jan. 1953, pp. 3–12.